(Received 27 April 2024, Accepted 16 July 2024, Scheduled 15 August 2024)

A Structured Basis to Determine Equivalent Dielectric Properties of Homogeneous Phantom Liquid Representing Multilayer Biological Tissues for SAR Measurement

Ardhendu Kundu[1,*], Kaushik Patra[2], Bhaskar Gupta[3], and Amirul I. Mallick[4]

[1] *Institute of Engineering & Management, University of Engineering & Management, Kolkata, West Bengal, India*
[2] *Bosch Global Software Technologies Pvt. Ltd., Bangalore, India*
[3] *Electronics and Telecommunication Engineering Department, Jadavpur University, Kolkata, West Bengal, India*
[4] *Department of Biological Sciences, Indian Institute of Science Education and Research Kolkata, West Bengal, India*

ABSTRACT: In today's era of wireless communication, interaction of electromagnetic energy and living biological systems is unavoidable — both in far field and in near field of the radiating antenna. Consequent basic safety limits on radiation levels are enforced through Specific Absorption Rate (SAR) limits. Practical measurement and validation of these SAR values require the deployment of phantom models containing tissue equivalent dielectric liquids — these liquids are conventionally single layer and homogeneous in nature. However, structured basis to formulate these custom made homogeneous phantom liquids representing arbitrary combinations of stacked tissue layers has not been properly reported in literature. To address the issue, this paper develops and illustrates a novel structured technique to define equivalent permittivity and loss tangent of homogeneous phantom liquid representing arbitrary combinations of stacked tissue layers — both in far field and in near field exposure scenarios. Electric field distribution and later on point SAR distribution inside different tissue layers have been attempted to replicate as closely as possible using equivalent homogeneous phantom liquid with properly tuned permittivity and loss tangent values. The fitting procedure involves minimization of the absolute/normalized maximum difference (of electric field and point SAR) between the original multilayer tissue and the modelled single layer homogeneous equivalent. This generalized technique is applied to two distinct multilayer (four layers are considered) biological models at 2.45 GHz where one is composed of four layers of equal thicknesses while the other one has four layers with unequal thicknesses. Moreover, the proposed technique has been tested and validated in the two abovementioned multilayer biological models for both far field (plane wave irradiation) and near field (in close proximity to antenna) exposure scenarios. This technique is quite successful in achieving equivalent dielectric liquids in which original point SAR data and its overall distribution across different layers can be realistically replicated while attempting point wise matching at several spatial points. In some cases, the original electric field/point SAR values are achieved with reduced precision near layer interfaces with significant dielectric contrast. Thus, the proposed technique can significantly contribute to accurately measure, validate, and reflect the true spatial SAR distributions in original multilayer biological models using the derived homogeneous tissue equivalent phantom liquids.

1. INTRODUCTION

Due to immense use of wireless communication systems over wide frequency spectrum, close interactions of electromagnetic energy and biological systems is unavoidable. This interaction mechanism can happen either in far field [1–8] or in near field [9–15] of the radiating structure depending upon applications. Living biological bodies are exposed to far field plane wave irradiation from cell tower antennas [1–8], whereas particularly the humans are exposed to near field emissions from cell phones and other body-centric electromagnetic devices [9–15]. Thus, the need to quantify electromagnetic energy absorption rate due to plane wave incidence is equally important as in cases of near field exposure close to the antenna. To quantify the amount of interaction in terms of electromagnetic energy, a term 'Specific Absorption Rate (SAR)' is coined in literature [16–20]; it is defined as the rate at which electromagnetic energy is absorbed per unit mass of a living biological prototype while it is exposed to an external electromagnetic field. SAR value depends upon shape of the living object, number of distinguishable layers, dielectric properties of individual layer, material density of each layer, and incident electric field strength [1–15]. With knowledge of these parameters, point SAR can be computed using standard electromagnetic solvers [21]. Mathematical expression for point SAR is $\sigma|E|^2/2\rho$ — where σ is the electrical conductivity of tissue, E the peak electric field strength developed inside tissue, and ρ the tissue density. Thus, point SAR largely depends on the second degree of peak electric field strength developed inside biological tissue — as a consequence, practical electric field probing inside biological prototype is an absolute requirement for SAR measurement. During practical measurement, invasive techniques involving insertion of electric field probes inside living biological tissue are avoided vide medical ethical guidelines. To circumvent this issue, attempts have been made to for-

* Corresponding author: Ardhendu Kundu (ardhendukundu.1989@gmail.com).

mulate and define an equivalent homogeneous liquid with predefined dispersive dielectric properties [10, 16, 18, 19, 22–25]. Initially, human head phantom liquid was proposed to be of average dielectric properties between grey matter and white matter for SAR measurement [10, 22, 23]. Later on, an equivalent dielectric liquid recipe was proposed based on an average of the permittivity of all tissue layers and tuning conductivity to match 1 g or 10 g averaged SAR value in specific model [24]. Similarly, another group proposed a set of head equivalent phantom liquids based on matching the maximum value of 10 g averaged SAR with tuned dielectric properties [25]. However, none of these techniques attempted to match the electric field or point SAR distribution inside original multilayered model and the equivalent homogeneous phantom liquid. Researchers are yet to address alignment of point SAR distributions between original multilayer model and equivalent homogeneous liquid on three dimensional basis. Moreover, SAR estimation in different plant and fruit models due to plane wave exposure (far field) is another contemporary research topic [1–8] — thus, multilayer plant/fruit tissues equivalent homogeneous phantom liquid formulation is an additional research challenge. To date, there is no generalized and structured framework to define dielectric properties of equivalent phantom liquid based on dielectric properties, thickness, stacking distribution, and geometric shape of original biological layers, and of course irrespective of far field or near field exposure scenarios. Consequently, there is dire need for a generalized technique to synthesize equivalent phantom liquids with customized permittivity and loss tangent for arbitrary combinations of stacked tissue layers either in far field or in near field exposure conditions. With SAR measurement being the primary objective, any chosen figure of merit for such synthesis should be based on realistic spatial matching of point-wise SAR or the electric field distributions internal to the biological structure.

This work aims at developing a novel generalized and structured technique to determine effective dielectric properties of homogenous liquid equivalent to a multilayer tissue models for accurate SAR measurement. Moreover, the proposed technique should accurately tune dielectric properties of the tissue equivalent liquid both in far field exposure scenario due to plane wave irradiation and in near field scenario, i.e., close to the transmitting antenna. Electric field and point SAR distributions in original multilayer model are taken into account while the basis towards structured technique is developed. Thickness, relative positioning, and geometric shape of each tissue layer are also considered while equivalent dielectric properties of the homogeneous phantom liquid are computed. The technique is developed in such a way that it works at any frequency of interest. Once developed, this technique is applied to two problems having four layers with different permittivity and loss tangent values. In one case, the layers are of equal thickness, and in the other, those are unequal. Furthermore, the proposed technique is applied on the above-mentioned multilayer biological models for both plane wave irradiation in far field scenario and in close proximity to transmitting antenna for testing near field scenario — thus, the generic nature of the novel technique is validated. Appropriate permittivity and loss tangent values for the multilayer tissue equivalent homogeneous phantom liquids are computed for two different tissue combinations and two exposure scenarios.

2. PROPOSED TECHNIQUE TO FORMULATE EQUIVALENT DIELECTRIC PROPERTIES OF MULTILAYER BIOLOGICAL BODY FOR SAR MEASUREMENT

Point SAR at a location inside biological tissue depends on the electric field strength developed at that point, electrical conductivity, and material density of the tissue.

Figure 1(a) illustrates the original problem composed of an n-layer (layer names L_1 to L_n, respectively) tissue model with respective layer thicknesses and material densities of z_1, z_2, z_3, ..., z_n and ρ_1, ρ_2, ρ_3, ..., ρ_n. All layers have equal dimensions along x ($-x/2$ to $+x/2$) and y ($-y/2$ to $+y/2$) axes and are of electrically large cross sections at the frequency of interest. Now, there are two possible exposure scenarios, i.e., either a far field plane wave passes through the n-layer tissue model or an antenna radiates in close proximity to the same n-layer tissue model. In far field exposure scenario, a linearly polarized plane wave with direction of propagation along z axis and electric field directed along x axis impinges on the first layer (L_1) and propagates through subsequent layers (L_2 to L_n, respectively). In the other case, a simple rectangular microstrip antenna radiates in fundamental mode along z axis (broadside direction) in close proximity (near field) of the first layer (L_1), and the fields further interact with the subsequent tissue layers, i.e., L_2 to L_n, respectively. Fig. 1(b) shows the equivalent homogeneous problem with single dielectric layer of permittivity ε_r, loss tan-

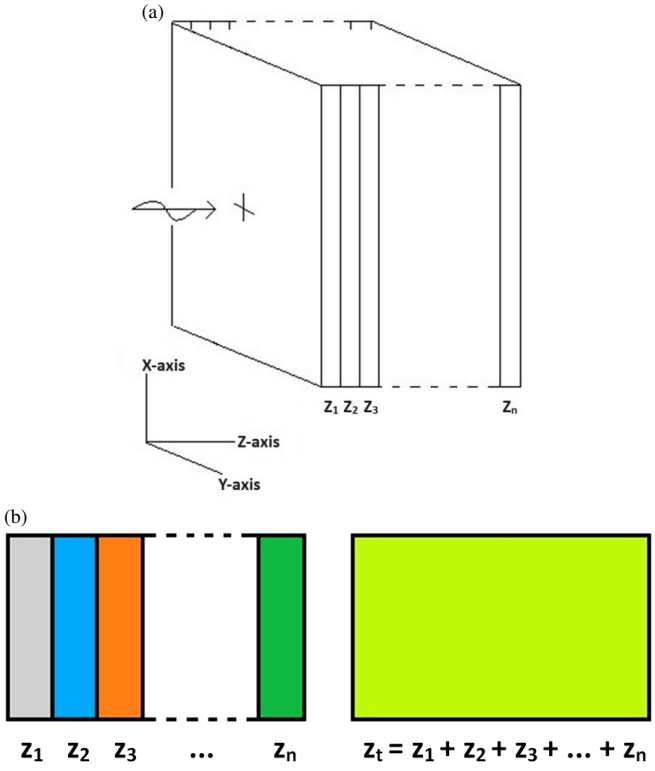

FIGURE 1. (a) Linearly polarized plane wave impinges on n-layer tissue model, and (b) equivalent homogeneous phantom model with single dielectric layer of thickness z_t.

gent tan δ, thickness z_t (where $z_t = z_1 + z_2 + z_3 + ... + z_n$), and material density ρ_e (depends upon choice of equivalent phantom medium based on original multilayer dielectric model). Primary objective is to find out ε_r and tan δ so that the electric field and point SAR distributions along central coordinate points ($x = 0$, $y = 0$, $z = 0$ to $z_1 + z_2 + z_3 + ... + z_n$) inside the multilayer model and the homogeneous model are spatially similar — however, the exactly same electric field and point SAR distributions cannot be attained using homogeneous liquid in particular around the original dielectric interfaces.

Initially, the maximum difference between the electric field distribution curves of the original n-layer model and equivalent phantom liquid with parametric permittivity and loss tangent is minimized. A position dependent (z dependent) cost function $f_{i(jk)}$ computed at ($x = 0$, $y = 0$) is defined as the absolute difference between two electric field distribution curves. This function is expressed as follows:

$$f_{i(jk)} = \left|E_{i(org)} - E_{i(jk)eq}\right| \tag{1a}$$

i varies from 0 to $z_1 + z_2 + z_3 + ... + z_n$

j represents tuned permittivity value

k represents tuned loss tangent value

Here, $E_{i(org)}$ and $E_{i(jk)eq}$ are respective magnitudes of peak electric fields at the ith location in original n-layer model and equivalent homogeneous phantom liquid.

Coordinate location at which $f_{i(jk)}$ is observed to be maximum, is unique for each combination of permittivity and loss tangent of the equivalent liquid. A figure of merit is defined as the maximum value of $f_{i(jk)}$, i.e., Max$(f_{i(jk)})$.

$$\text{Figure of merit} = \text{Max}(f_{i(jk)}) \tag{1b}$$

This requires to be minimized by tuning effective permittivity (j) and loss tangent (k) of equivalent homogeneous phantom liquid.

In the case of the original multilayer problem, the magnitude of electric field is usually maximum in the first layer (L_1) and is large compared to subsequent layers (L_2 to L_n, respectively). Consequently, the figure of merit definition in (1b) is dominated by the first layer itself, and the eventual equivalent dielectric properties are biased toward the L_1 characteristics — very little priority is assigned to the subsequent layers. To overcome this anomaly, a modified figure of merit is defined based on maximum fractional difference between electric field distribution curves of original n-layer model and equivalent homogeneous phantom liquid. This new basis would avoid unnecessary priority allotted to initial layers. A new z-coordinate dependent dimensionless function $f'_{i(jk)}$ at ($x = 0$, $y = 0$) is introduced in (2a) as

$$f'_{i(jk)} = \left|\left(E_{i(org)} - E_{i(jk)eq}\right)/E_{i(org)}\right| \tag{2a}$$

Modified figure of merit is defined as the maximum value of $f'_{i(jk)}$, i.e., Max$(f'_{i(jk)})$.

$$\text{Figure of merit} = \text{Max}(f'_{i(jk)}) \tag{2b}$$

Next, the basis is further revised in view of taking care of direct difference in point SAR distribution rather than peak electric field distribution. Point SAR varies with squared magnitude of electric field strength developed inside biological tissue layers (SAR $= \sigma|E|^2/2\rho$ where σ is the tissue conductivity, E the peak electric field developed inside tissue layer, and ρ the tissue density). It is argued that a formulation framework based on point SAR would be more appropriate than using the electric field directly as SAR is the standard metric to correlate with electromagnetic energy absorption rate in biological objects. Consequently, a different function ($g_{i(jk)}$) at ($x = 0$, $y = 0$) is introduced as the absolute difference between two point SAR distribution curves for different coordinate points on z axis. Figure of merit is defined as the maximum value of $g_{i(jk)}$, i.e., Max$(g_{i(jk)})$,and the same needs to be minimized.

$$g_{i(jk)} = \left|\text{point SAR}_{i(org)} - \text{point SAR}_{i(jk)eq}\right| \tag{3a}$$

$$\text{Figure of merit} = \text{Max}(g_{i(jk)}) \tag{3b}$$

During the final stage, maximum fractional difference between two point SAR distribution curves (at $x = 0$, $y = 0$) is minimized for finalizing dielectric properties of the equivalent homogeneous phantom liquid.

$$g'_{i(jk)} = \left|\left(\text{point SAR}_{i(org)} - \text{point SAR}_{i(jk)eq}\right) / \text{point SAR}_{i(org)}\right| \tag{4a}$$

This figure of merit is defined as maximum value of dimensionless function $g'_{i(jk)}$, i.e., Max$(g'_{i(jk)})$.

$$\text{Figure of merit} = \text{Max}(g'_{i(jk)}) \tag{4b}$$

It should be noted that the proposed technique is generalized for any number of layers, individual layer thickness, dielectric properties of each layer, material density of each layer, frequency of operation, far field as well as near field exposure, incident electric field strength, and shape of multilayer biological object.

3. MULTILAYER EQUIVALENT DIELECTRIC PROPERTIES OF HOMOGENEOUS PHANTOM LIQUID FOR PLANE WAVE EXPOSURE IN FAR FIELD SCENARIO

3.1. A Typical Four Layer Model with Equal Layer Thickness (Plane Wave Exposure)

The proposed technique outlined in the last section is now applied to a four layer (L_1 to L_4) tissue model with different permittivity and loss tangent values but with identical individual layer thicknesses. Moreover, it is assumed that all layers possess equal material density of 1000 kg/m^3. A linearly polarized plane wave at 2.45 GHz impinges on the designed four equal layers model. The plane wave impinges on the first layer (L_1) with normal incidence and thereafter, propagates through three subsequent layers (L_2 to L_4). Incident plane wave has peak electric field strength of 27.46 V/m as prescribed in Indian public exposure scenario [17]. Individual layers are of 50 cm by 50 cm cross section with 1 cm thickness each (as illustrated in

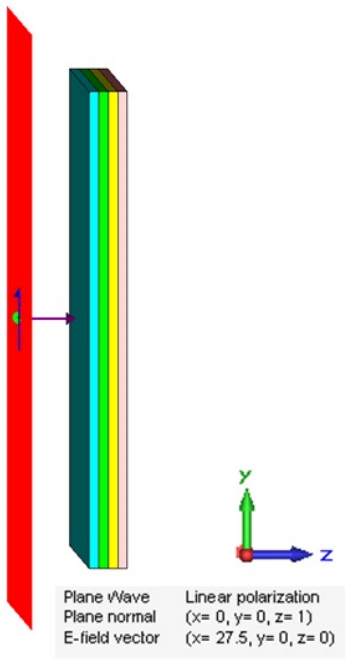

FIGURE 2. A linearly polarized plane wave at 2.45 GHz impinges on four equal layer tissue model having different dielectric properties.

Fig. 2). Peak electric field/point SAR data have been noted at centre of each layer ($x = 0$, $y = 0$) to ensure negligible effect of boundary discontinuity along lateral directions. Thickness and dielectric properties of each layer are given in Table 1. A time domain simulation is performed to obtain peak electric field/point SAR distributions at ($x = 0$, $y = 0$) of original four equal layers model in CST MWS 2018 [21]. Thereafter, seventy two subsequent simulations have been performed by varying the homogeneous phantom liquid permittivity from 20 to 75, loss tangent from 0.10 to 0.35 with fixed material density of 1000 kg/m^3. Finally, the proposed technique in step by step basis has been applied to derive equivalent dielectric properties of homogeneous phantom liquid for SAR measurement.

TABLE 1. Thickness and dielectric properties of four equal layers model.

Layer	Permittivity at 2.45 GHz	Loss tangent at 2.45 GHz
L_1: 0–1 cm	30	0.30
L_2: 1–2 cm	45	0.25
L_3: 2–3 cm	60	0.20
L_4: 3–4 cm	75	0.15

3.1.1. Brief Description of Computational Electromagnetic Simulation Setup

High contrast in dielectric properties of adjacent layers and low quality factor of lossy dielectric layers are two primary reasons to choose transient solver for proper meshing of the multilayer structure illustrated in Fig. 2. Transient solver in CST MWS 2018 [21] works based on Finite Integration Technique computational scheme, and the same was conceptualized in 1977 [26, 27]. In the solution space, Maxwell's integral equations are discretized and solved using numerical technique. The multilayer structure has been discretized using hexahedral cells of variable sizes where a wavelength in dielectric layers is divided into twenty segments. In boundary settings, four perfectly matched layers with 0.0001 reflection coefficient are set as absorbing boundary. Steady state energy criterion of -40 dB is chosen for inverse transformation to monitor frequency domain features.

3.1.2. Results and Discussion on Equivalent Phantom Liquid for the Typical Four Equal Layer Model (Plane Wave Exposure)

Results, in this section, demonstrate how successfully the proposed technique derives effective dielectric properties of homogeneous phantom liquid equivalent to the above mentioned four equal tissue layer model considering far field plane wave exposure scenario for practical electric field/SAR measurements in phantom model. Based on the findings, it is noted that minimizing the maximum percentage difference in electric field/point SAR distributions between the four equal layers model and equivalent single homogeneous phantom liquid model fits best for the purpose.

Figures of merit defined in (1)–(4) are utilized to determine the permittivity and loss tangents of the phantom liquid equivalent to the four equal layer problem — due to linearly polarized plane wave exposure at 2.45 GHz.

First, the figure of merit definition of (1a) and (1b) is taken up. Fig. 3(a) illustrates Max$(f_{i(jk)})$ plot for varied permittivity and loss tangent of equivalent phantom liquid. Observation indicates that permittivity and loss tangent of (50, 0.20) produce a peak electric field distribution that is closest to that of original four equal layers model. Figs. 3(b) and 3(c) illustrate the comparison of peak electric field distribution curves along with absolute difference plot for (50, 0.20) combination. Maximum difference of 1.46 V/m between peak electric field distribution curves is noted in the third layer (L_3) at (0, 0, 2.96 cm) location.

Next, equivalent dielectric properties of the phantom liquid are derived using (2a) and (2b). Fig. 3(d) illustrates Max$(f'_{i(jk)})$ plot for varied permittivity and loss tangent of the equivalent phantom liquid. Dielectric properties of (40, 0.35) produce a peak electric field distribution that is closest to that of original four equal layers model while minimizing the maximum percentage difference. Figs. 3(e) and 3(f) illustrate the comparison of peak electric field distributions w.r.t original four equal layers model along with difference plot for (40, 0.35) combination. A maximum difference of 1.91 V/m between peak electric field distribution curves is noted in the first layer (L_1) at (0, 0, 0.66 cm) coordinate.

With SAR measurement being the primary target, dielectric properties of the equivalent liquid are now computed using the metric defined in (3a) and (3b). Maximum difference in point SAR distribution over ($x = 0$, $y = 0$, $z = 0$ to 4 cm) coordinates is minimized. Fig. 4(a) illustrates Max$(g_{i(jk)})$ plot against varied permittivity and loss tangent of equivalent phantom liquid for SAR measurement. Dielectric properties of (25, 0.30) produce point SAR distribution closest to original four equal layer model. Figs. 4(b) and 4(c) illustrate the compari-

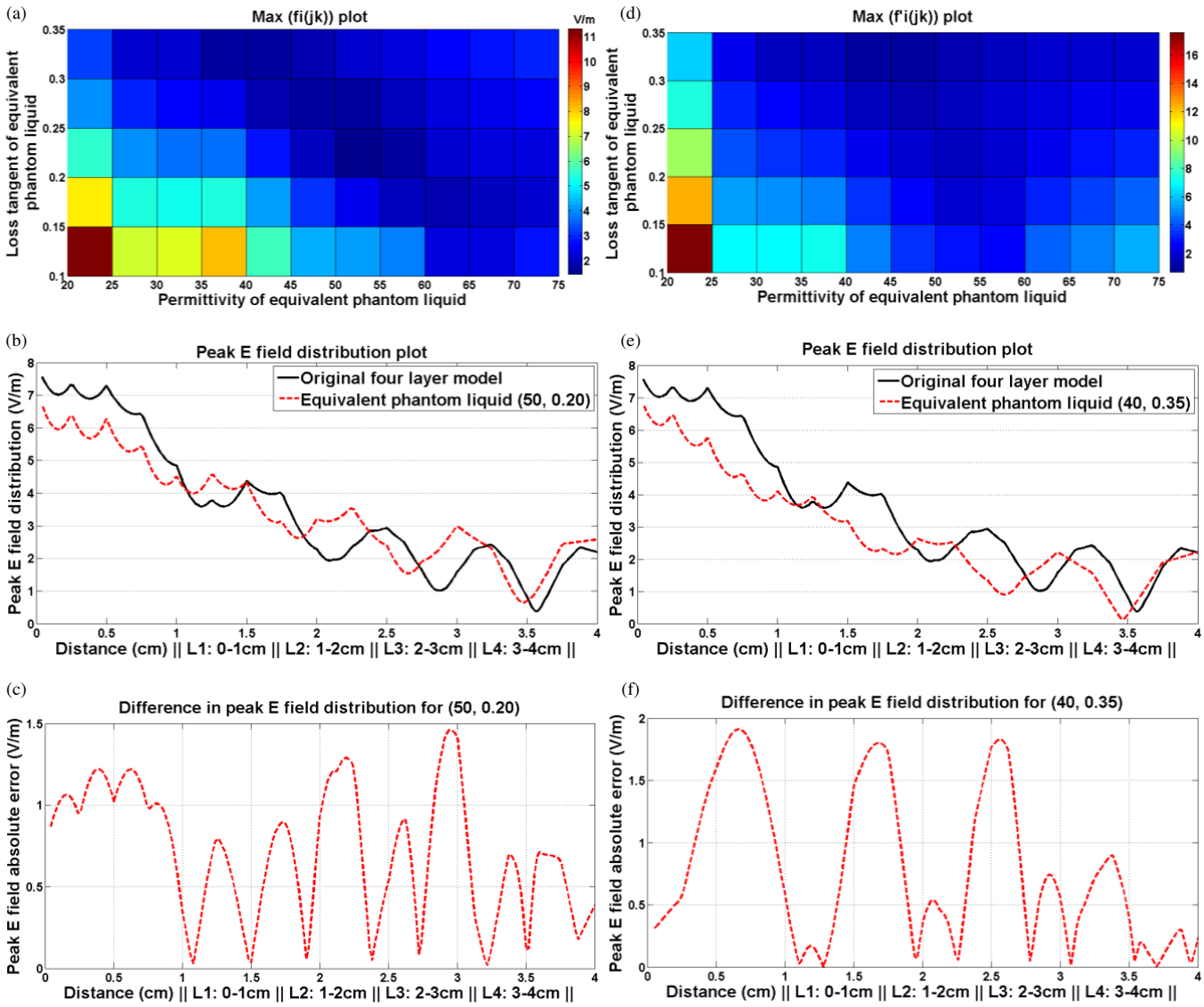

FIGURE 3. Four equal layers model — plane wave exposure in far field scenario. (a) Max($f_{i(jk)}$) plot for varied permittivity and loss tangent of equivalent model, (b) comparison of electric field distributions between four equal layers model and equivalent dielectric properties (50, 0.20) that lead to smallest Max($f_{i(jk)}$), (c) difference in peak E field distribution for equivalent dielectric properties (50, 0.20), (d) Max($f'_{i(jk)}$) plot for varied permittivity and loss tangent of equivalent model, (e) comparison of electric field distributions between four equal layers model and equivalent dielectric properties (40, 0.35) that result in smallest Max($f'_{i(jk)}$), (f) difference in peak E field distribution for equivalent dielectric properties (40, 0.35).

son of point SAR distributions along with point SAR difference plot for (25, 0.30) combination. It is noted that point SAR distribution inside derived equivalent dielectric liquid (25, 0.30) is best matched in the first layer (L_1) of original four equal layers model (refer to Fig. 4(b)). However, the obtained difference in overall point SAR distribution is also one order down compared to the original four equal layers model as observed in Fig. 4(c). A maximum difference of 1.9×10^{-3} W/kg in point SAR is observed at the interface of second (L_2) and third (L_3), i.e., at (0, 0, 2 cm) coordinate.

At last, final attempt is made to closely replicate point SAR distribution not only in the first layer (L_1) but also in subsequent layers (L_2 to L_4) by minimizing normalized SAR distribution over ($x = 0$, $y = 0$, $z = 0$ to 4 cm) coordinates. (4a) and (4b) have been employed on raw data sets to minimize the maximum percentage difference in point SAR distribution because of replacing four equal layers model with a single homogeneous phantom liquid. Fig. 4(d) illustrates Max($g'_{i(jk)}$) plot for different combinations of permittivity and loss tangent of the equivalent phantom liquid to measure SAR accurately. Dielectric properties of (40, 0.35) produce a point SAR distribution over ($x = 0$, $y = 0$, $z = 0$ to 4 cm) coordinates that is well replicated and similar to original four equal layers model based on (4a) and (4b). Figs. 4(e) and 4(f) depict comparison of point SAR distributions and difference in point SAR distribution plot for (40, 0.35) combination. It is noted that point SAR distribution inside derived equivalent liquid dielectric (40, 0.35) is well matched over second to fourth layers (L_2 to L_4) too rather than

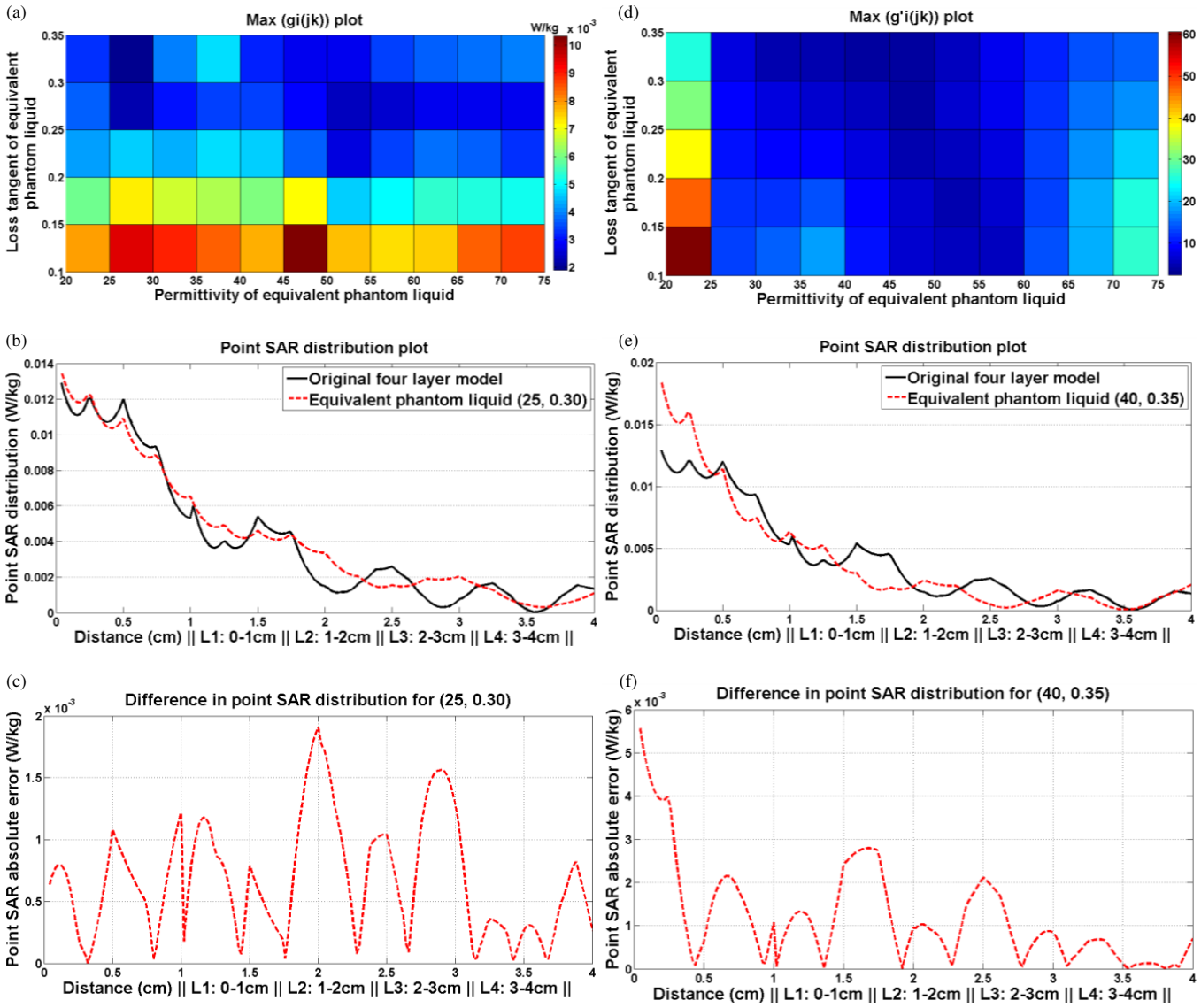

FIGURE 4. Four equal layers model — plane wave exposure in far field scenario. (a) Max$(g_{i(jk)})$ plot for varied permittivity and loss tangent of equivalent model, (b) comparison of point SAR distributions between four layer model and equivalent dielectric properties (25, 0.30) that lead to smallest Max$(g_{i(jk)})$, (c) difference in point SAR distribution for equivalent dielectric properties (25, 0.30), (d) Max$(g'_{i(jk)})$ plot for varied permittivity and loss tangent of equivalent model, (e) comparison of point SAR distributions between four layer model and equivalent dielectric properties (40, 0.35) that result in smallest Max$(g'_{i(jk)})$, (f) difference in point SAR distribution for equivalent dielectric properties (40, 0.35).

only in the first layer (L_1) (refer to Fig. 4(e)). However, the obtained difference in overall point SAR distribution is still one order down compared to original four equal layers model as observed in Fig. 4(f). A maximum difference of 5.6×10^{-3} W/kg in point SAR is observed at the open surface of first layer (L_1), i.e., at (0, 0, 0) coordinate.

3.2. A Typical Four Layer Model with Unequal Layer Thickness (Plane Wave Exposure)

All the steps and observations are now repeated for a multilayer tissue model with four unequal layers (L_1 to L_4) possessing different permittivity and loss tangent. Contrast in dielectric properties is exactly similar to that stated for earlier model whereas all layers possess material density of 1000 kg/m^3. A linearly polarized plane wave at 2.45 GHz impinges on the first layer (L_1) with normal incidence and propagates through subsequent layers (L_2 to L_4). Incident plane wave possesses peak electric field strength of 27.46 V/m [17]. All layers are of 50 cm by 50 cm cross section but of unequal thickness. Individual layer thickness and dielectric properties are tabulated in Table 2. Time domain simulation is performed to note peak electric field/point SAR distribution inside original four unequal layers model in CST MWS 2018 [21]. Peak electric field/point SAR data have been noted at ($x = 0$, $y = 0$, $z = 0$ to 2.5 cm) coordinates of four layers to ensure negligible effect of boundary discontinuity except at layer interfaces. Thereafter, seventy two more simulations have been performed by varying equivalent homo-

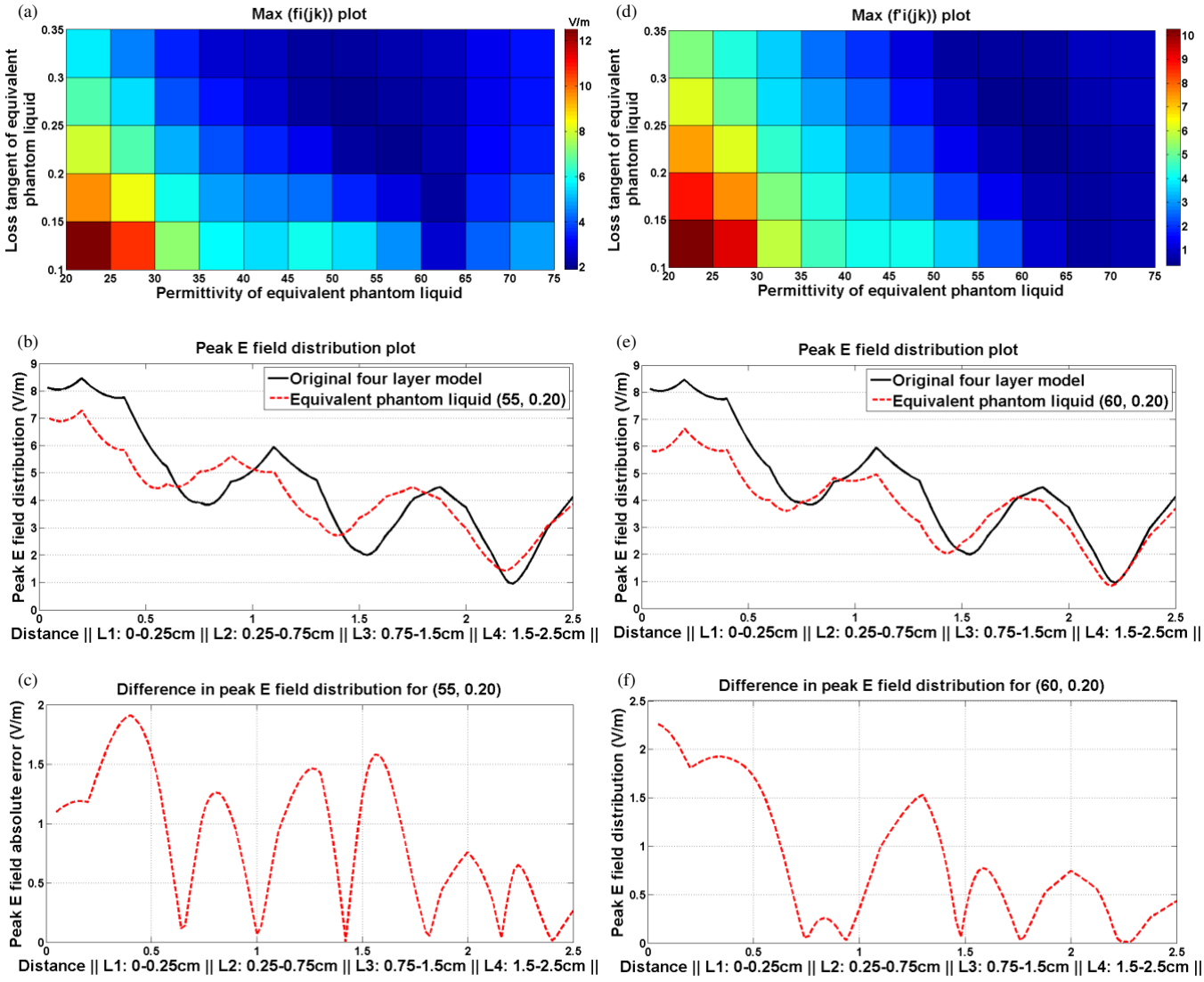

FIGURE 5. Four unequal layers model — plane wave exposure in far field scenario. (a) Max$(f_{i(jk)})$ plot for varied permittivity and loss tangent of equivalent model, (b) comparison of electric field distributions between four unequal layers model and equivalent dielectric properties (55, 0.20) that lead to smallest Max$(f_{i(jk)})$, (c) difference in peak E field distribution for equivalent dielectric properties (55, 0.20), (d) Max$(f'_{i(jk)})$ plot for varied permittivity and loss tangent of equivalent model, (e) comparison of electric field distributions between four unequal layers model and equivalent dielectric properties (60, 0.20) that result in smallest Max$(f'_{i(jk)})$, (f) difference in peak E field distribution for equivalent dielectric properties (60, 0.20).

geneous phantom permittivity from 20 to 75, loss tangent from 0.10 to 0.35, and fixed material density of 1000 kg/m^3. At last, the proposed technique has been deployed in step by step manner to determine equivalent dielectric properties of equivalent phantom liquid for SAR measurement.

3.2.1. Results and Discussion on Equivalent Phantom Liquid for the Typical Four Layer Model with Unequal Layer Thickness (Plane Wave Exposure)

Similar to earlier observations, results for the four unequal layer model also endorse that the proposed technique efficiently formulates effective dielectric properties of equivalent homogeneous phantom liquid for practical electric field/SAR measurement considering far field plane wave exposure scenario. Once again, it is observed that minimizing the maximum percentage difference in electric field/point SAR distributions between the original four unequal layers model and equivalent single homogeneous phantom liquid model fits well.

TABLE 2. Thickness and dielectric properties of four unequal layers model.

Layer	Permittivity at 2.45 GHz	Loss tangent at 2.45 GHz
L_1: 0–0.25 cm	30	0.30
L_2: 0.25–0.75 cm	45	0.25
L_3: 0.75–1.50 cm	60	0.20
L_4: 1.50–2.50 cm	75	0.15

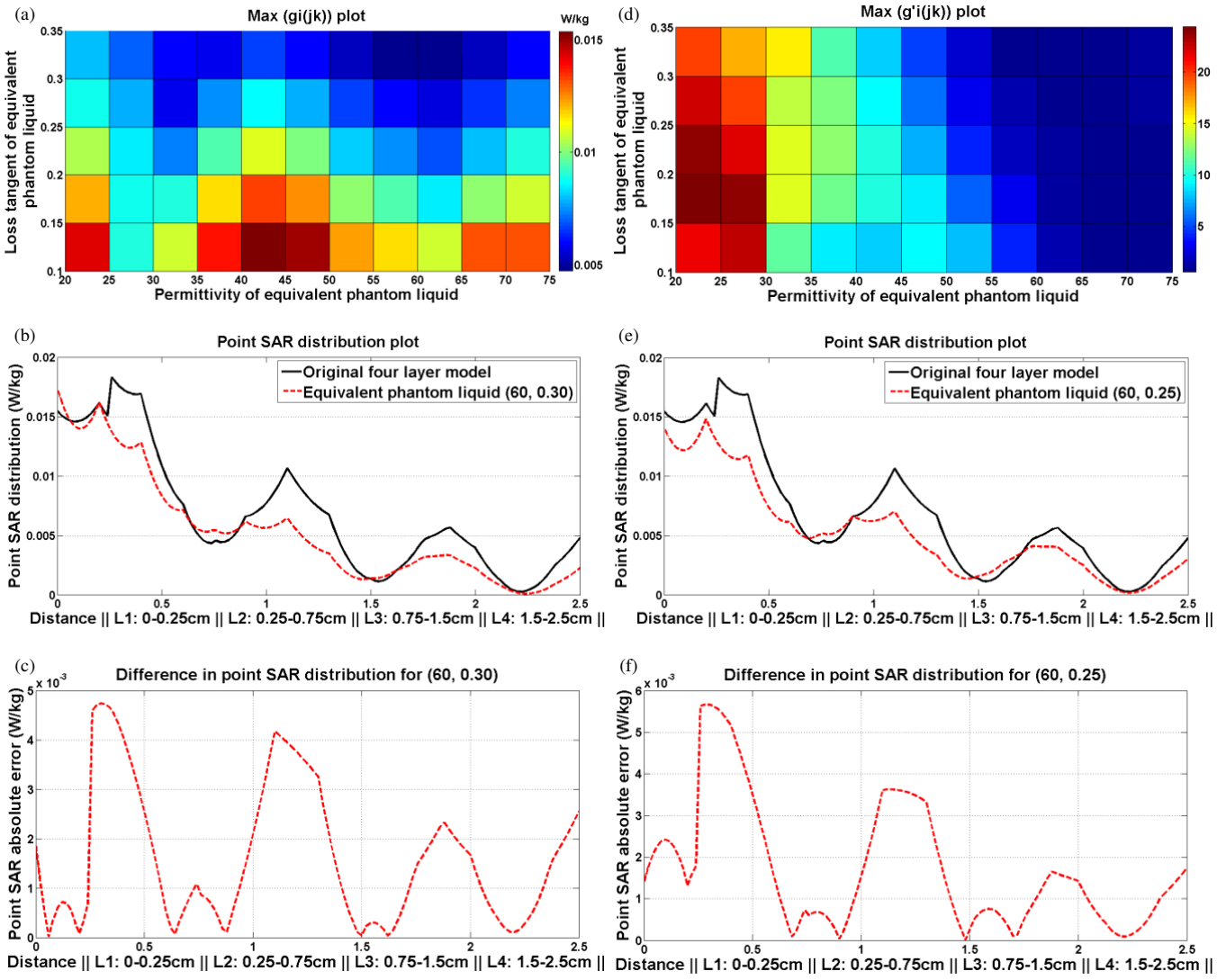

FIGURE 6. Four unequal layers model — plane wave exposure in far field scenario. (a) Max$(g_{i(jk)})$ plot for varied permittivity and loss tangent of equivalent model, (b) comparison of point SAR distributions between four layer model and equivalent dielectric properties (60, 0.30) that lead to smallest Max$(g_{i(jk)})$, (c) difference in point SAR distribution for equivalent dielectric properties (60, 0.30), (d) Max$(g'_{i(jk)})$ plot for varied permittivity and loss tangent of equivalent model, (e) comparison of point SAR distributions between four layer model and equivalent dielectric properties (60, 0.25) that result in smallest Max$(g'_{i(jk)})$, (f) difference in point SAR distribution for equivalent dielectric properties (60, 0.25).

The four metrics defined in (1)–(4) are applied here as well to estimate the permittivity of the proposed equivalent dielectric liquid — obtained results are discussed next. Firstly, (1a)–(1b) are utilized to observe and predict the phantom properties by tuning permittivity and loss tangent. Fig. 5(a) illustrates Max$(f_{i(jk)})$ plot for varied permittivity and loss tangent of equivalent phantom liquid. It is observed that permittivity and loss tangent of (55, 0.20) reproduce a peak electric field distribution closest to the original unequal layers model. Figs. 5(b) and 5(c) depict comparison of peak electric field distributions along with absolute difference plot for (55, 0.20) combination. The observed maximum difference between peak electric field distribution curves is 1.91 V/m in the second layer (L_2) at (0, 0, 0.40 cm) location.

Next, metrics defined in (2a)–(2b) are employed. Fig. 5(d) illustrates Max$(f'_{i(jk)})$ plot for varied permittivity and loss tangent of equivalent phantom liquid. Dielectric properties of (60, 0.20) produce a peak electric field distribution closest to original four unequal layers model while minimizing normalized difference of overall peak electric field distribution. Figs. 5(e) and 5(f) depict the comparison of peak electric field distributions along with difference plot for (60, 0.20) combination. A maximum of 2.26 V/m difference in peak electric field distribution is still observed in the first layer (L_1) at (0, 0, 0.04 cm) coordinate.

Next, the figure of merit based on point SAR ((3a) and (3b)) distribution over ($x = 0$, $y = 0$, $z = 0$ to 2.5 cm) coordinates is minimized to obtain the equivalent phantom properties. Fig. 6(a) illustrates Max$(g_{i(jk)})$ plot for different combinations

of permittivity and loss tangent of equivalent phantom liquid for unequal layers model. Equivalent dielectric properties of (60, 0.30) reproduce a point SAR distribution closest to original unequal layer model based on protocol defined in (3a)–(3b). Figs. 6(b) and 6(c) depict the comparison of point SAR distributions along with point SAR difference plot for (60, 0.30) combination. It should be noted that point SAR distribution inside equivalent dielectric liquid (60, 0.30) is best matched in the first layer (L_1) of original four unequal layers model (refer to Fig. 6(b)). The observed difference in overall point SAR distribution inside equivalent phantom liquid is one order down compared to original four unequal layers model (refer to Fig. 6(c)). A maximum difference of 4.74×10^{-3} W/kg in point SAR is observed in the second layer (L_2) at (0, 0, 0.30 cm) coordinate.

In the end, dielectric properties of the phantom liquid is determined using the metric defined in (4a)–(4b). This involves the normalized point SAR at ($x = 0$, $y = 0$, $z = 0$ to 2.50 cm). Fig. 6(d) illustrates Max$(g'_{i(jk)})$ plot for different combinations of permittivity and loss tangent of equivalent phantom liquid. Dielectric properties of (60, 0.25) produce point SAR distribution over ($x = 0$, $y = 0$, $z = 0$ to 2.50 cm) coordinates that is closest to original point SAR distribution in four unequal layers model based on Equations (4a) and (4b). Figs. 6(e) and 6(f) illustrate the comparison of point SAR distributions and difference in point SAR distributions for (60, 0.25) combination. It is observed that point SAR distribution inside derived equivalent dielectric liquid (60, 0.25) is better matched over the second to fourth layers (L_2 to L_4) compared to earlier protocol described above (refer to Fig. 6(e)). Moreover similar to earlier case, the difference in overall point SAR distribution is one order down compared to original unequal layers model as seen in Fig. 6(f). A maximum difference of 5.65×10^{-3} W/kg in point SAR is observed in the starting of second layer (L_2), i.e., at (0, 0, 0.30 cm) coordinate.

4. MULTILAYER EQUIVALENT DIELECTRIC PROPERTIES OF HOMOGENEOUS PHANTOM LIQUID CLOSE TO THE RADIATING ANTENNA IN NEAR FIELD SCENARIO

4.1. A Typical Four Layer Model with Equal Layer Thickness (In Close Proximity to Antenna)

This time, a simple rectangular microstrip patch antenna radiates at 2.45 GHz in fundamental mode along z axis (broadside direction) in close proximity (near field) to the first layer (L_1) of the same four equal tissue layer model (L_1 to L_4) — the fields further interact with the subsequent tissue layers, i.e., L_2 to L_4 (refer to Fig. 7). Next, the earlier proposed technique is applied to the four equal tissue layer model (L_1 to L_4) and specifications of the individual layers are as described in Section 3 (refer to Table 1). Antenna radiated power in near field first impinges on the first layer (L_1) with normal incidence and then further interacts with the subsequent layers, i.e., L_2 to L_4. The average input power of the antenna has been set at 0.50 Watt — thus, the electric field/point SAR values shouldn't be compared with earlier case of linearly polarized plane wave irradiation. The peak electric field/point SAR data have been noted

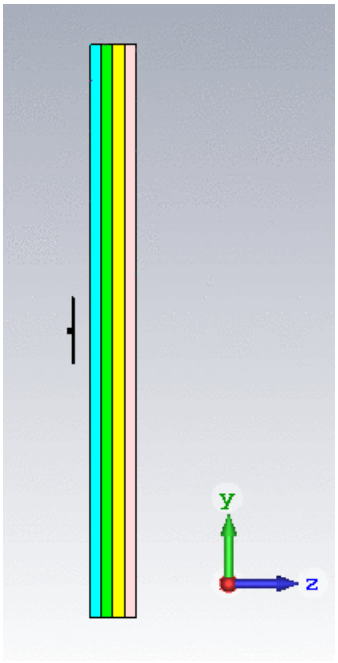

FIGURE 7. A rectangular microstrip antenna radiates at 2.45 GHz in close proximity to the four equal layer tissue model having different dielectric properties.

along central coordinates ($x = 0$, $y = 0$, $z = 0$ to 4 cm) of the original four equal layers model using time domain simulation. The same electromagnetic simulation setup has been followed in CST MWS 2018 as stated earlier [21]. Afterwards, seventy two subsequent simulations have been run with varied permittivity (20 to 75) and loss tangent (0.10 to 0.35) along with a fixed material density of 1000 kg/m^3 of the equivalent homogeneous phantom liquid. At last, the earlier proposed technique has been applied to determine the dielectric properties of the closest equivalent phantom liquid for SAR measurement.

4.1.1. Results and Discussion on Equivalent Phantom Liquid for the Typical Four Equal Layer Model (In Close Proximity to Antenna)

Results endorse that the proposed technique derives effective dielectric properties of equivalent homogeneous phantom liquid for the above mentioned four equal tissue layer model not only in far field but also in close proximity to the radiating antenna, i.e., in near field exposure scenario.

Once again, prescribed figures of merit in (1)–(4) are employed to determine the permittivity and loss tangent of equivalent homogeneous phantom liquid — due to 2.45 GHz near field radiation in close proximity to the antenna.

At first, Fig. 8(a) illustrates Max$(f_{i(jk)})$ plot for varied permittivity and loss tangent of equivalent phantom liquid — employing the figure of merit defined using (1a) and (1b). It is observed that permittivity and loss tangent of (30, 0.35) produce a peak electric field distribution closest to the original four equal layers model. Figs. 8(b) and 8(c) illustrate the comparison of peak electric field distribution curves and the absolute difference plot for (30, 0.35) combination. A maximum difference of 18.54 V/m between the peak electric field distribution

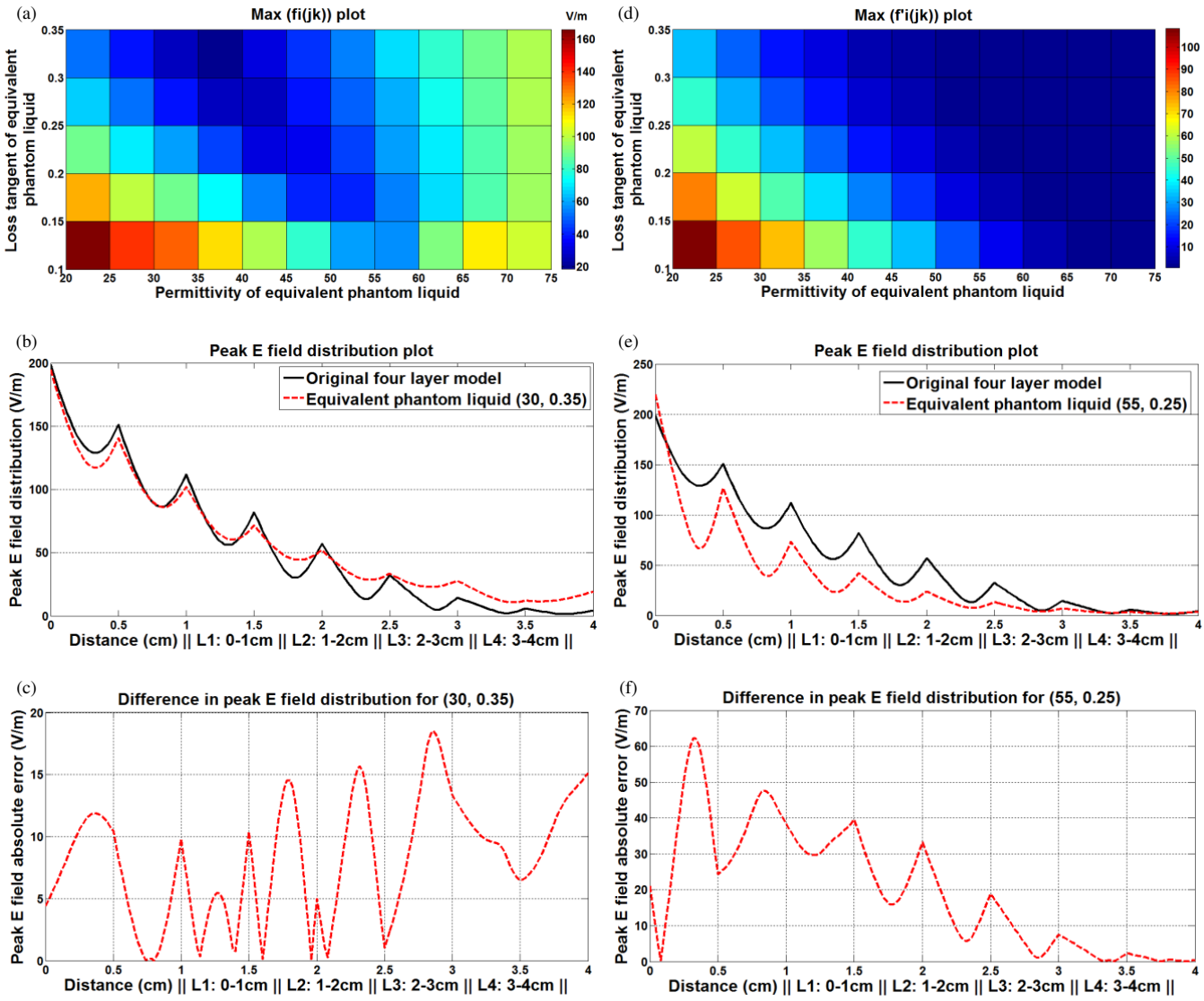

FIGURE 8. Four equal layers model — close to the radiating antenna in near field scenario. (a) Max$(f_{i(jk)})$ plot for varied permittivity and loss tangent of equivalent model, (b) comparison of electric field distributions between four equal layers model and equivalent dielectric properties (30, 0.35) that lead to smallest Max$(f_{i(jk)})$, (c) difference in peak E field distribution for equivalent dielectric properties (30, 0.35), (d) Max$(f'_{i(jk)})$ plot for varied permittivity and loss tangent of equivalent model, (e) comparison of electric field distributions between four equal layers model and equivalent dielectric properties (55, 0.25) that result in smallest Max$(f'_{i(jk)})$, (f) difference in peak E field distribution for equivalent dielectric properties (55, 0.25).

curves is noted in the third layer (L_3) at (0, 0, 2.86 cm) location.

Subsequently, equivalent dielectric properties of homogeneous liquid are derived using (2a) and (2b). Fig. 8(d) illustrates Max$(f'_{i(jk)})$ plot for a wide range of permittivity and loss tangent values of the equivalent liquid. Finally, dielectric properties of (55, 0.25) produce the peak electric field distribution closest to original four equal layers model — while, minimizing the maximum percentage difference. Figs. 8(e) and 8(f) illustrate the comparison of peak electric field distributions w.r.t original four equal layers model and also the difference plot for (55, 0.25) combination. This time, a large maximum electric field difference is noted in the first layer (L_1) at (0, 0, 0.34 cm) coordinate.

Next, the maximum difference in point SAR distribution over ($x = 0$, $y = 0$, $z = 0$ to 4 cm) coordinates is attempted to minimize employing the metric defined in (3a) and (3b). Fig. 9(a) illustrates Max$(g_{i(jk)})$ plot for the above mentioned ranges of permittivity and loss tangent of the equivalent phantom liquid for SAR measurement. Dielectric properties of (30, 0.30) produce a point SAR distribution over central coordinates of the four layers ($x = 0$, $y = 0$, $z = 0$ to 4 cm) that closely replicates the point SAR distribution in the original four equal layers model. Figs. 9(b) and 9(c) illustrate the comparison of point SAR distributions along with the point SAR difference

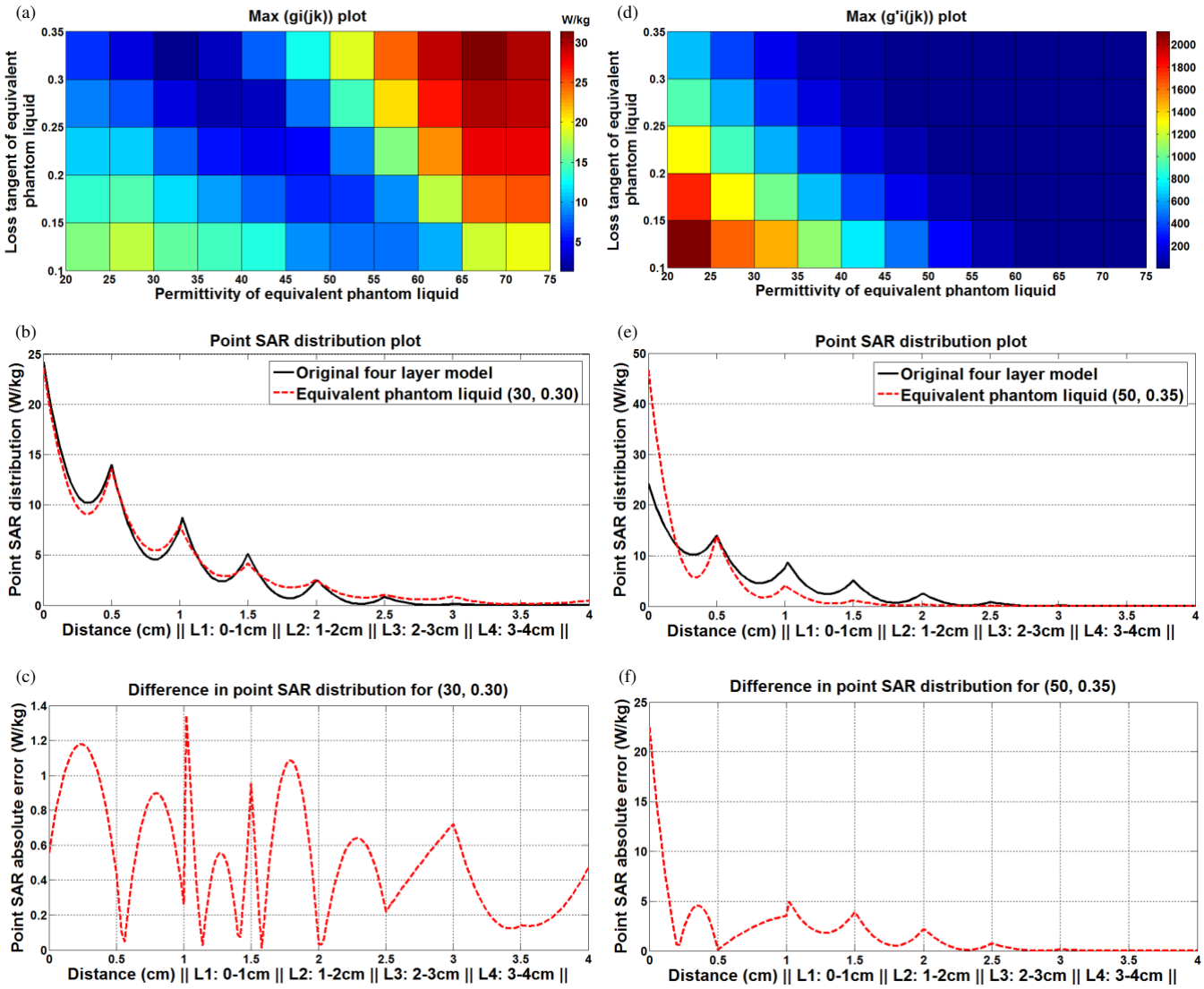

FIGURE 9. Four equal layers model — close to the radiating antenna in near field scenario. (a) Max$(g_{i(jk)})$ plot for varied permittivity and loss tangent of equivalent model, (b) comparison of point SAR distributions between four layer model and equivalent dielectric properties (30, 0.30) that lead to smallest Max$(g_{i(jk)})$, (c) difference in point SAR distribution for equivalent dielectric properties (30, 0.30), (d) Max$(g'_{i(jk)})$ plot for varied permittivity and loss tangent of equivalent model, (e) comparison of point SAR distributions between four layer model and equivalent dielectric properties (50, 0.35) that result in smallest Max$(g'_{i(jk)})$, (f) difference in point SAR distribution for equivalent dielectric properties (50, 0.35).

plot for (30, 0.30) combination. The point SAR distribution inside derived equivalent homogeneous liquid (30, 0.30) is well matched over all the four layers (L_1 to L_4) (refer to Fig. 9(b)). Noted difference in overall point SAR distribution is quite negligible compared to the original four equal layers model — as, noted in Fig. 9(c). A maximum difference of 1.34 W/kg in point SAR is observed in the second layer (L_2), i.e., at (0, 0, 1.02 cm) coordinate.

In the final attempt, (4a) and (4b) have been employed to minimize the maximum percentage difference in point SAR distribution across all four equal layers (L_1 to L_4). Thus, the normalized SAR distribution is attempted to minimize over ($x = 0$, $y = 0$, $z = 0$ to 4 cm) coordinates. Fig. 9(d) illustrates Max$(g'_{i(jk)})$ plot for different combinations of permittivity and loss tangent of the equivalent homogeneous phantom liquid. Dielectric properties of (50, 0.35) produce point SAR distribution closest to the original four equal layers model. Figs. 9(e) and 9(f) depict comparison of point SAR distributions along with their difference plot for (50, 0.35) combination. Point SAR distribution inside the derived equivalent dielectric liquid (50, 0.35) is reasonably matched in all four equal layers (L_1 to L_4) except at the open interface of the very first layer (L_1) — please refer to Figs. 9(e) and 9(f).

4.2. A Typical Four Layer Model with Unequal Layer Thickness (In Close Proximity to Antenna)

Now, the rectangular microstrip patch antenna at 2.45 GHz fundamental mode radiates along z axis in close proximity to the first layer (L_1) of four unequal tissue layer model (L_1 to L_4) and

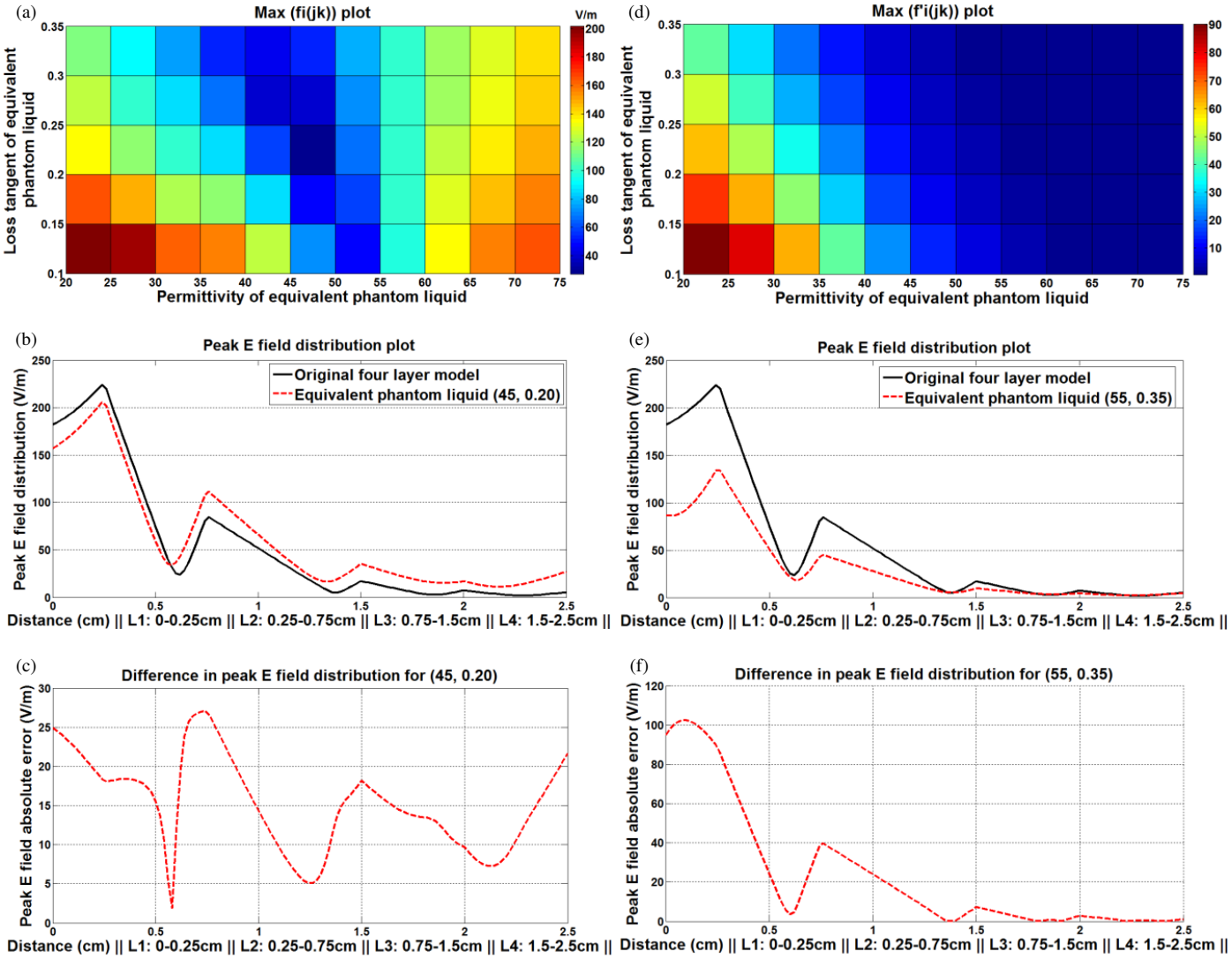

FIGURE 10. Four unequal layers model — close to the radiating antenna in near field scenario. (a) Max($f_{i(jk)}$) plot for varied permittivity and loss tangent of equivalent model, (b) comparison of electric field distributions between four unequal layers model and equivalent dielectric properties (45, 0.20) that lead to smallest Max($f_{i(jk)}$), (c) difference in peak E field distribution for equivalent dielectric properties (45, 0.20), (d) Max($f'_{i(jk)}$) plot for varied permittivity and loss tangent of equivalent model, (e) comparison of electric field distributions between four unequal layers model and equivalent dielectric properties (55, 0.35) that result in smallest Max($f'_{i(jk)}$), (f) difference in peak E field distribution for equivalent dielectric properties (55, 0.35).

the radiated fields further interact with subsequent tissue layers, i.e., L_2 to L_4. The thickness and dielectric properties of each layer are as described in Table 2 — moreover, dielectric contrast among four layers is exactly the same as stated earlier and all tissue layers possess material density of 1000 kg/m^3. Next, the above mentioned steps are once again applied to the four unequal tissue layers model. Here also, the average input power of antenna has been kept 0.50 Watt — the peak electric field/point SAR data have been noted along central coordinates ($x = 0$, $y = 0$, $z = 0$ to 2.5 cm) of the four unequal layers. Next, seventy two additional simulations have been performed over wide ranges of permittivity (20 to 75) and loss tangent (0.10 to 0.35) of the equivalent homogeneous phantom liquid. At the end, dielectric properties of the equivalent phantom liquid have been determined for SAR measurement in the four unequal layers model.

4.2.1. Results and Discussion on Equivalent Phantom Liquid for the Typical Four Layer Model with Unequal Layer Thickness (In Close Proximity to Antenna)

Similar to previous observations, once again, results endorse that the formulated technique well derives effective dielectric properties of equivalent homogeneous phantom liquid for the above mentioned four unequal tissue layer model in near field exposure scenario, i.e., in close proximity to the antenna.

Figures of merit defined in (1)–(4) have been applied again to estimate dielectric properties of the equivalent homogeneous phantom liquid — noted results are discussed below.

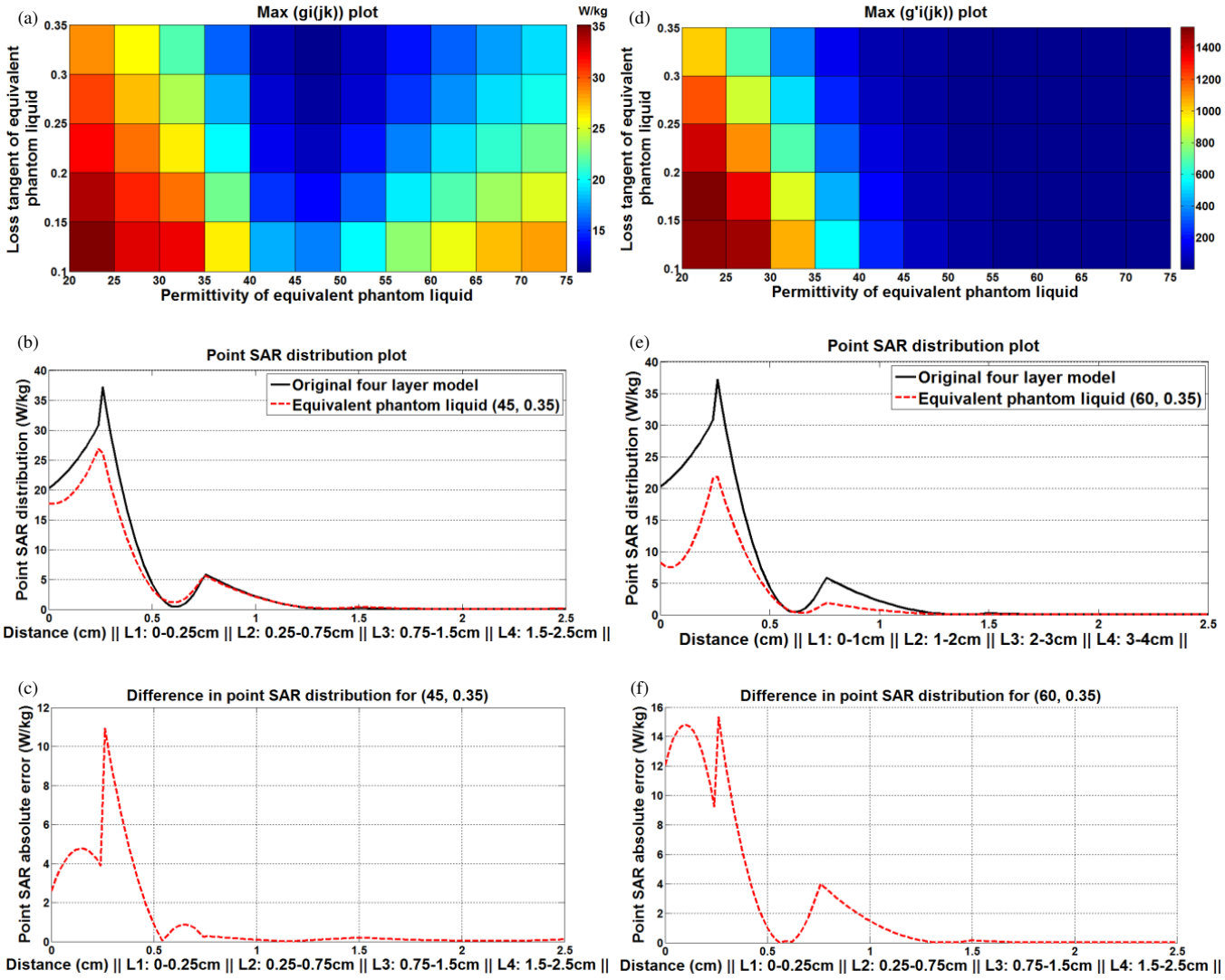

FIGURE 11. Four unequal layers model — close to the radiating antenna in near field scenario. (a) Max$(g_{i(jk)})$ plot for varied permittivity and loss tangent of equivalent model, (b) comparison of point SAR distributions between four layer model and equivalent dielectric properties (45, 0.35) that lead to smallest Max$(g_{i(jk)})$, (c) difference in point SAR distribution for equivalent dielectric properties (45, 0.35), (d) Max$(g'_{i(jk)})$ plot for varied permittivity and loss tangent of equivalent model, (e) comparison of point SAR distributions between four layer model and equivalent dielectric properties (60, 0.35) that result in smallest Max$(g'_{i(jk)})$, (f) difference in point SAR distribution for equivalent dielectric properties (60, 0.35).

Figure of merit defined using (1a)–(1b) has been utilized — consequently, Fig. 10(a) demonstrates Max$(f_{i(jk)})$ plot for wide ranges of permittivity and loss tangent of the equivalent homogeneous phantom liquid. Specific combination of permittivity and loss tangent (45, 0.20) produces a peak electric field distribution closest to the original four unequal layers model. Figs. 10(b) and 10(c) illustrate the comparison of peak electric field distributions and the absolute difference plot for (45, 0.20) combination. Noted maximum difference between peak electric field distribution curves is 27.08 V/m near the interface of second (L_2) and third (L_3) layers at (0, 0, 0.74 cm) location.

Subsequently, metrics defined in (2a)–(2b) are employed in the next step — Fig. 10(d) depicts Max$(f'_{i(jk)})$ plot for the same ranges of permittivity and loss tangent of the equivalent homogeneous liquid. Dielectric properties of (55, 0.35) finally reproduce peak electric field distribution closest to the original four unequal layers model while minimizing normalized difference of overall peak electric field distribution. Figs. 10(e) and 10(f) demonstrate the comparison of peak electric field distributions and the difference plot for (55, 0.35) combination. However, still a significantly large maximum electric field difference is noted in the first layer (L_1) at (0, 0, 0.08 cm) coordinate.

Thereafter, the proposed figure of merit based on point SAR ((3a) and (3b)) distribution is attempted to minimize — Fig. 11(a) demonstrates Max$(g_{i(jk)})$ plot for wide ranges of permittivity and loss tangent of the equivalent phantom liquid for four unequal layers model. Final equivalent dielectric properties of (45, 0.35) produce point SAR distribution close to the original unequal layers model. Figs. 11(b) and 11(c) illustrate respectively the comparison of point SAR distributions

TABLE 3. Comparison of proposed technique with the past reported work.

Reported work	Biological model	Technique to define Dielectric Properties of equivalent phantom liquid for SAR measurement	Can this technique match spatial SAR distribution?	Remarks
[10]	Human head	Average dielectric properties of all brain tissues	No	Only maximum 1 g or 10 g averaged SAR values are matched, unable to replicate spatial SAR distributions
[22]	Human head	Average dielectric properties of grey matter and white matter in brain	No	Volume-averaged peak SAR can be matched with slight over-estimation, unable to replicate spatial SAR distributions
[23]	Human head	Average dielectric properties of grey matter and white matter in brain	No	Volume-averaged peak SAR can be matched, unable to replicate spatial SAR distributions
[24]	Human head	Average permittivity of all tissue layers and tuning conductivity to match 1 g or 10 g averaged SAR value in specific model	No	Volume-averaged (1 g or 10 g) peak SAR values can be matched, unable to replicate spatial SAR distributions
[25]	Human head	Based on matching the maximum value of 10 g averaged SAR with tuned dielectric properties	No	Volume-averaged (10 g) peak SAR values can be matched, unable to replicate spatial SAR distributions
This work	Any multilayer biological model	Based on two (or three) dimensional spatial matching of point-wise SAR (or electric field) distribution irrespective of far field or near field exposure scenario	Yes	Local point or volume-averaged spatial SAR distribution can be matched — able to replicate spatial SAR distributions on three dimensional coordinate basis

and the point SAR difference plot for (45, 0.35) combination. It is observed that point SAR distribution inside the equivalent dielectric liquid (45, 0.35) is sensibly matched with the original model — however, a reasonable difference is observed at and around the interface of first (L_1) and second (L_2) layers at (0, 0, 0.26 cm) coordinate.

At last, Fig. 11(d) illustrates the Max($g'_{i(jk)}$) plot for wide ranges of permittivity and loss tangent of equivalent phantom liquid employing the metrics defined in (4a)–(4b) — it involves minimizing the maximum value of normalized point SAR. Dielectric properties of (60, 0.35) produce a point SAR distribution over ($x = 0$, $y = 0$, $z = 0$ to 2.50 cm) coordinates close to the original point SAR distribution in four unequal layers model. Figs. 11(e) and 11(f) demonstrate the comparison of point SAR distributions and their difference for (60, 0.35) combination. It is observed that the nature of point SAR distribution inside the equivalent homogeneous dielectric liquid (60, 0.35) is matched with the original unequal layers model — please refer to Figs. 11(e) and 11(f). However, a considerable difference is still observed in the first (L_1) and second (L_2) layers with peak near the interface of those two layers at (0, 0, 0.26 cm) coordinate.

5. DISCUSSIONS

It should be noted that minimizing the maximum fractional difference in point SAR distribution provides the appropriate dielectric properties of the equivalent phantom liquid for most of the multilayer tissue models while targeting overall SAR measurement in all the layers. Thus, the overall original SAR distribution along with individual SAR values is replicated with minimum possible errors. Even in some cases, minimizing the absolute maximum point SAR difference results in achieving appropriate equivalent dielectric phantom liquid for SAR measurement in multilayer models. However, it must also be noted that even the derived equivalent homogeneous liquid to some extent lacks in precisely replicating the original electric field/point SAR values near layer interfaces with significant dielectric contrast. This disagreement in electric field/point SAR data near layer interfaces cannot be avoided entirely using homogeneous phantom liquid because the reflection and re-

fraction of electromagnetic wave at layer interfaces can only take place in multilayer model with dielectric discontinuities — these phenomena do not occur in equivalent homogeneous phantom liquid. The proposed technique can more accurately derive equivalent dielectric properties of any arbitrary shaped multilayer tissue model in case raw simulation data is available for each and every point inside the layers of that arbitrarily shaped model instead of only at central coordinate points, i.e., ($x = 0$, $y = 0$, $z = 0$ to $z_1 + z_2 + z_3 + ... + z_n$). In addition, special attention can also be emphasized on any specific tissue layer (in multilayer model) where the most accurate electric field/SAR measurement is an absolute necessity — dielectric properties of the equivalent homogeneous phantom liquid can accordingly be tuned. Thus, the proposed technique to determine equivalent dielectric properties of the homogeneous phantom liquid is much improved compared to earlier reported techniques available in literature [10, 16, 22–25]. Table 3 lists how the proposed technique is better than the past work in determining multilayer equivalent homogeneous phantom liquid dielectric properties for practical SAR measurements.

6. CONCLUSIONS

This work contributes to significant advancement in the domain of formulating equivalent phantom properties by developing a novel, generalized and structured technique that does not merely attempt to match the maximum SAR value, rather it attempts to replicate overall geometric peak electric field/point SAR distribution inside equivalent phantom liquid similar to the original multilayer biological model. This is a more appropriate metric than matching averaged SAR data over 1 g or 10 g contiguous mass since once point SAR distribution is matched inside equivalent liquid, all other SAR data either averaged over 1 g or 10 g contiguous mass would match well with original multilayer model. As verified for two different four layers models both in far-field and in close proximity to antenna, peak electric field/point SAR distribution inside derived equivalent phantom liquid matches exactly at multiple coordinate points in different tissue layers, and the overall peak electric field or point SAR distribution patterns are also quite well replicated using proposed technique (except at layer interfaces). It is observed that the basis of using normalized point SAR (i.e., fractional difference in point SAR distribution) provides appropriate dielectric properties of the homogeneous phantom liquid in most cases of SAR measurements. Furthermore, practical realization of equivalent homogeneous phantom model along with subsequent measurements would provide additional confidence. Equivalent homogeneous phantom liquids are in the process of development with de-ionized water, sucrose, sodium chloride, and bactericide to attain target dielectric properties — once developed, spatial point SAR distribution can be measured.

It should also be pointed out that exact point by point matching of point SAR distribution across different layers can never be achieved using a single homogeneous equivalent dielectric liquid because of the absence of dielectric discontinuities unlike the original multilayer tissue model. However, procedure outlined in this work presents an optimal solution as it minimizes the worst case scenario, i.e., maximum mismatch between the original problem formulation and the equivalent model. Hence, the developed technique can be adopted by electromagnetic regulatory organizations to prescribe equivalent dielectric properties for customized multilayer biological body during practical SAR measurement.

ACKNOWLEDGEMENT

Authors would like to acknowledge lab members for their constructive criticisms and suggestions to improve this work. BG acknowledges RUSA 2.0 scheme (Govt. of India) for providing research grant support.

REFERENCES

[1] Kundu, A., "Specific absorption rate evaluation in apple exposed to RF radiation from GSM mobile towers," in *2013 IEEE Applied Electromagnetics Conference (AEMC)*, 1–2, KIIT, Bhubaneswar, India, 2013.

[2] Kundu, A. and B. Gupta, "Comparative SAR analysis of some Indian fruits as per the revised RF exposure guideline," *IETE Journal of Research*, Vol. 60, No. 4, 296–302, 2014.

[3] Kundu, A., B. Gupta, and A. I. Mallick, "SAR analysis in a typical bunch of grapes exposed to radio frequency radiation in Indian scenario," in *2016 International Conference on Microelectronics, Computing and Communications (MicroCom)*, 1–5, NIT Durgapur, West Bengal, India, 2016.

[4] Kundu, A., B. Gupta, and A. I. Mallick, "Specific absorption rate evaluation in a typical multilayer fruit: Coconut with twig due to electromagnetic radiation as per Indian standards," *Microwave Review*, Vol. 23, No. 2, 24–32, 2017.

[5] Kundu, A., B. Gupta, and A. I. Mallick, "Dependence of electromagnetic energy distribution inside a typical multilayer fruit model on direction of arrival and polarization of incident field," in *2019 IEEE Radio and Antenna Days of the Indian Ocean (RADIO)*, 1–2, Reunion, France, 2019.

[6] Kundu, A., B. Gupta, and A. I. Mallick, "Contrast in specific absorption rate for a typical plant model due to discrepancy among global and national electromagnetic standards," *Progress In Electromagnetics Research M*, Vol. 99, 139–152, 2021.

[7] Mukherjee, N., A. Kundu, and M. Mitra, "Study of SAR data and spatial distribution in a peace lily plant model under different electromagnetic exposure scenarios," *Progress In Electromagnetics Research C*, Vol. 136, 61–74, 2023.

[8] Kundu, A., B. Gupta, and A. I. Mallick, "Role of power density, frequency, direction of arrival and polarization of incident field on specific absorption rate distribution inside a multilayer fruits model," *Progress In Electromagnetics Research B*, Vol. 105, 123–136, 2024.

[9] Stuchly, S. S., M. A. Stuchly, A. Kraszewski, and G. Hartsgrove, "Energy deposition in a model of man: Frequency effects," *IEEE Transactions on Biomedical Engineering*, Vol. 33, No. 7, 702–711, 1986.

[10] Meier, K., V. Hombach, R. Kastle, R. Y.-S. Tay, and N. Kuster, "The dependence of electromagnetic energy absorption upon human-head modeling at 1800 MHz," *IEEE Transactions on Microwave Theory and Techniques*, Vol. 45, No. 11, 2058–2062, 1997.

[11] Cooper, J., B. Marx, J. Buhl, and V. Hombach, "Determination of safety distance limits for a human near a cellular base station antenna, adopting the IEEE standard or ICNIRP guidelines,"

Bioelectromagnetics, Vol. 23, No. 6, 429–443, 2002.

[12] Christ, A., A. Klingenbock, T. Samaras, C. Goiceanu, and N. Kuster, "The dependence of electromagnetic far-field absorption on body tissue composition in the frequency range from 300 MHz to 6 GHz," *IEEE Transactions on Microwave Theory and Techniques*, Vol. 54, No. 5, 2188–2195, 2006.

[13] Bačová, F. and M. Beňová, "The specific absorption rate of 10 g and 1 g methods comparison for a child and an adult in a shielded space of railway compartment," in *2023 24th International Conference on Computational Problems of Electrical Engineering (CPEE)*, 1–4, Grybów, Poland, 2023.

[14] Yu, S.-W., X. Zhang, Q.-S. Wu, L. Zhu, T. Yuan, and Q.-H. Jiang, "Low-SAR and high-FBR patch antenna with small ground size for wearable devices," *IEEE Open Journal of Antennas and Propagation*, Vol. 5, No. 1, 124–129, 2024.

[15] Kodera, S., K. Taguchi, Y. Diao, T. Kashiwa, and A. Hirata, "Computation of whole-body average SAR in realistic human models from 1 to 100 GHz," *IEEE Transactions on Microwave Theory and Techniques*, Vol. 72, No. 1, 91–100, 2024.

[16] Means, D. L. and K. W. Chan, "Evaluating compliance with FCC guidelines for human exposure to radiofrequency electromagnetic fields — Additional information for evaluating compliance of mobile and portable devices with FCC limits for human exposure to radiofrequency emissions: Supplement C edition 01-01 to OET Bulletin 65 edition 97-01," Office of Engineering and Technology, Federal Communications Commission, 2001, https://transition.fcc.gov/bureaus/oet/info/documents/bulletins/-oet65/oet65c.pdf [Last accessed 14 February 2024].

[17] DoT (Department of Telecommunications), "A journey for EMF," 2012, https://dot.gov.in/journey-emf [Last accessed 25 March 2024].

[18] IEC/IEEE International Standard, "Determining the peak spatial-average specific absorption rate (SAR) in the human body from wireless communications devices, 30 MHz to 6 GHz — Part 1: General requirements for using the finite-difference time-domain (FDTD) method for SAR calculations," *IEC/IEEE 62704-1*, 1–86, 2017, https://webstore.iec.ch/publication/34411.

[19] IEC/IEEE International Standard, "Determining the peak spatial-average specific absorption rate (SAR) in the human body from wireless communications devices, 30 MHz to 6 GHz — Part 2: Specific requirements for finite difference time domain (FDTD) modelling of exposure from vehicle mounted antennas," *IEC/IEEE 62704-2*, 1–112, 2017, https://webstore.iec.ch/publication/31306.

[20] ICNIRP (International Commission on Non-Ionizing Radiation Protection), "Guidelines for limiting exposure to electromagnetic fields (100 kHz to 300 GHz)," *Health Physics*, Vol. 118, No. 5, 483–524, 2020.

[21] CST MWS 2018 (CST Studio Suite® 2018), https://www.3ds.com/products/simulia/cst-studio-suite [Last accessed 25 March 2024].

[22] Hombach, V., K. Meier, M. Burkhardt, E. Kuhn, and N. Kuster, "The dependence of EM energy absorption upon human head modeling at 900 MHz," *IEEE Transactions on Microwave Theory and Techniques*, Vol. 44, No. 10, 1865–1873, 1996.

[23] Meier, K., M. Burkhardt, T. Schmid, and N. Kuster, "Broadband calibration of E-field probes in lossy media [mobile telephone safety application]," *IEEE Transactions on Microwave Theory and Techniques*, Vol. 44, No. 10, 1954–1962, 1996.

[24] Drossos, A., V. Santomaa, and N. Kuster, "The dependence of electromagnetic energy absorption upon human head tissue composition in the frequency range of 300–3000 MHz," *IEEE Transactions on Microwave Theory and Techniques*, Vol. 48, No. 11, 1988–1995, 2000.

[25] Monebhurrun, V., C. Dale, J.-C. Bolomey, and J. Wiart, "A numerical approach for the determination of the tissue equivalent liquid used during SAR assessments," *IEEE Transactions on Magnetics*, Vol. 38, No. 2, 745–748, 2002.

[26] Weiland, T., "A discretization model for the solution of Maxwell's equations for six-component fields," *Archiv für Elektronik und Uebertragungstechnik*, Vol. 31, 116–120, 1977.

[27] Clemens, M. and T. Weiland, "Discrete electromagnetism with the finite integration technique," *Progress In Electromagnetics Research*, Vol. 32, 65–87, 2001.